Vol.3, No.9, 750-767 (2011)
http://dx.doi.org/10.4236/ns.2011.39100

Natural Science

K-Ar age, geochemical, and Sr-Pb Isotopic compositions of keban magmatics, elaziğ, Eastern Anatolia, Turkey

Sevcan Kürüm

Engineering Faculty, Department of Geology, University of Fırat, Elazig, Turkey; skurum@firat.edu.tr

Received 9 August 2011; revised 11 September 2011; accepted 27 September 2011.

ABSTRACT

Keban magmatics consist of plutonic rocks of acidic and intermediate compositions with different phases. They are the equivalent of surface rocks. In the current study on plutonic rocks, general petrographic features, disequilibrium textures such as skeletal formation in minerals, poikilitic texture, oscillatory zoning, and mineral fragmentation, and growth states are observed. Besides these microscopic properties, the existence of rounded mafic enclaves of various sizes, petrographic syn-plutonic dykes, and field data support the idea that mafic and felsic magmas are mixed. Keban magmatics have I-type, metaluminous-peraluminous characteristics. Diorites and quartz diorites have low-K tholeiitic features, whereas tonalites have low-K calc-alkaline features. Compared with diorites, tonalites are richer in terms of LREE (Rock/Chondrite); Rb, Sr, and Ba (LILE); and Hf, Zr, Th, and U (HFSE) elements. LILE enrichment, which signals the crustal contamination of mantle-originated magmas, is particularly observable in tonalites. In both rock groups, the negative anomaly of Nb is a sign of similarity of pluton to the subduction zone magma series. Based on the K-Ar geochronology dating of amphibole minerals, the ages of these rocks are found to be 75.65 ± 1.5 and 59.77 ± 1.2 Ma in tonalites and 84.76 ± 1.8 and 84.35 ± 1.7 Ma in diorite and quartz diorites. The $^{87}Sr/^{86}Sr$ isotope ratios in tonalites are 0.705405 and 0.706053, whereas these ratios are 0.704828 and 0.704754 in dioritic rocks. Pb isotope ratios are similar in both rock types.

Keywords: Keban Magmatics, K-Ar Age; Pb-Sr Isotopes; Geochemistry

1. INTRODUCTION

Within the Southeastern Anatolia orogenic belt and the Neotethys convergent system developed during the tectonomagmatic evolution of the southern Neotethys, Keban magmatics form the easternmost branch of the Göksun-Afşin, Doğanşehir, and Baskil granitoids [1-8] (**Figure 1**). These granitoids of the Cretaceous age [3,6] have intrusive contact relationships [3-7,11-13] with platform carbonates (Malatya-Keban metamorphic), ophiolites (Göksun, İspendere, Kömürhan, Guleman), metamorphic rocks related to ophiolites (Berit) [6,7,14], and ensimatic island-arc units present in the orogenic belt (Elazığ-Yüksekova) [3,4,6,7,11,12,15].

The objective of the current paper is to present the field relations, petrography, geochemical and isotopic (Sr-Pb) composition, and K-Ar hornblende ages of Keban magmatics. The study contributes in determining the location of these rocks within Cretaceous plutonic rocks spread throughout southeast Anatolia and in establishing geodynamic evolution in future regional studies.

2. ANALYTICAL TECHNIQUES

Thin section sample preparation and crushing and grinding to obtain whole-rock powders were performed at the laboratories of the Department of Geological Engineering, Firat University, Elaziğ, Turkey.

Whole-rock chemical analyses have been performed at the ACME laboratories and at the ACT-labs by ICP-AES (major and some trace elements) and ICP-MS (some trace and rare earth elements, REE) in Canada; Mineral separates for K-Ar analyses were extracted by conventional procedures including grinding, sieving and heavy liquid separation. K-Ar age determination of mineral separates consisting of amphibole ± biotite and pure amphibole has been performed at the K-Ar Geochronology Laboratory, Geological Survey of Israel, Jerusalem, Israel. For K determination, two aliquots of ca. 0.25 g were taken from a sample and dissolved using

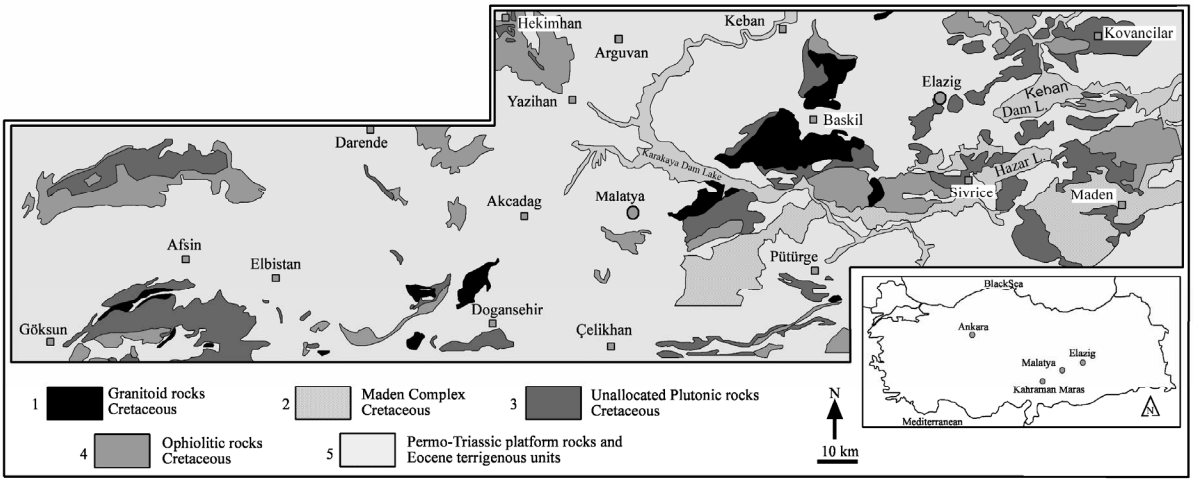

Figure 1. Simplified map of the Cretaceous units of the area between Göksum (Kahramanmaras) and Kovancilar (Elazig) (from [9,10]).

lithium metaborate ($LiBO_2$). Potassium concentrations were measured on ICP-AES (Perkin Elmer OPTIMA 3300) along with repeated determinations of three of the international standards SO-3, BE-N, BHVO-1, SCo-1, NIM-L, NIM-G. The 1σ uncertainty for the K concentration of duplicates was less than 3%. The argon analysis for K-Ar determination was performed using the standard isotope dilution procedures routinely used in the geochronological laboratory at the GSI [16,17]. About 0.03 g sample was loaded into the glass arm of a metal extraction line and heated overnight at 120˚C. Argon was extracted in a molybdenum crucible using RF induction heating. Gases were scrubbed through liquid nitro gen and Zr Al getters. Argon was measured on a VG MM-1200 mass spectrometer. Measured intensities were corrected for linear extrapolation of the ^{40}Ar peak and then $^{i}Ar/^{39}Ar$ ratios (i = other isotopes). Argon was measured in duplicates and uncertainties are reported at the 1σ level.

Sr and Pb isotopic analyses were performed at the Mineralogical Institute of Heidelberg University, Germany.

3. GEOLOGICAL SETTING

The study area is situated in the Southeast Anatolia Orogenic Belt. This belt was formed by the collision of the Afro-Arabian and Eurasian plates following the oceanic closure of the south Tethyan in the Cretaceous-Miocene era [6,7]. This orogenic belt, which stretches from east to west, consists of three different zones [6,12, 18] and is divided into two nap zones: lower and upper [12]. The lower nap zone is made up of ophiolitic units, and the upper nap zone consists of Malatya Keban metamorphic massives [6,12,19]. The granitoids in Maraş, Malatya, and Elazığ regions, which formed during the evolution of southern Neotethys, have intrusive contact relationships with metamorphic massives (Malatya-Keban metamorphites), ensimatic island-arc units (Elazığ magmatic rocks/Yüksekova complex), ophiolitic rocks (Göksun, İspendere, Kömürhan, Guleman), and metamorphic rock units related to ophiolites (Berit) [7,8,10]. Malatya-Keban metamorphic massives and ophiolitic units were tectonically placed prior to the intrusions formed in the late Cretaceous period [3,13,20].

The geological units in the study area begin with the Keban metamorphic rocks from the Paleozoic-Mesozoic age. Keban metamorphic rocks are composed of marble, schist, and phyllites [21,22]; they crop out along the south-north direction in the western parts of the study area (**Figure 2**). One of the researcher [21] suggested that these rocks of carbonate and pelitic origin have low P-T conditions and that they underwent metamorphism during the Jurassic-lower Cretaceous era. The other researchers [23,24] pointed out that the metamorphism of the Malatya-Keban platform limestones is related to tectonism and asserted that these tectonic events caused by subduction still emerged on the edge of an active continent during the Senonian era. Thus, he concluded that metamorphism of limestones and tectonism is contemporaneous. Conversely, some researchers [2,4] proposed that the P and T conditions that caused the metamorphism of the Keban metamorphics are related to the northerly subduction of the oceanic crust located south of the Keban unit in the upper Cretaceous rocks and to the formation of the Elazığ magmatic rocks formed above this subduction zone. Contact metamorphism (skarnitization) is observed along intrusive contacts between metamorphic and plutonic rocks [24,25]. Palaeocene-Oligocene sedimentary rocks unconformably overlaid all the metamorphics, ophiolites, intrusive, and volcano-sedimentary rocks in the study area.

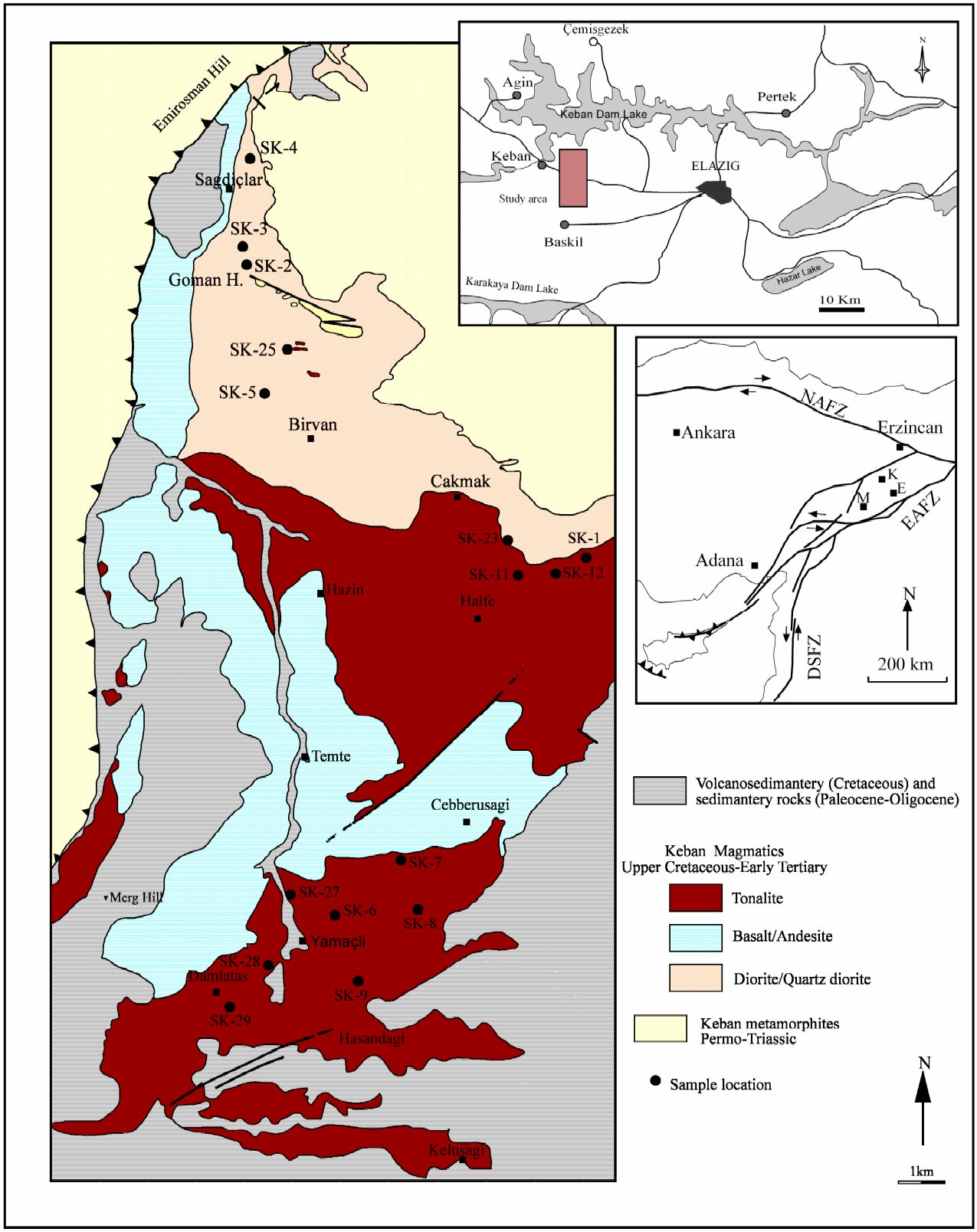

Figure 2. Geological map of the Keban magmatic rocks (taken from [4]) and location map of the study area. M: Malatya; E: Elazig; K: Keban; Erz: Erzincan; DSFZ: Dead Sea Fault Zone; EAFZ: East Anatolian Fault Zone; NAFZ: North Anatolian Fault Zone.

The thrust fault between the Keban metamorphics and the Keban pluton forms the main tectonic structure in the study area (**Figure 2**).

4. FIELD OBSERVATIONS AND PETROGRAPHY

Late Cretaceous-Palaeocene Keban magmatic rocks were mapped as tonalite, diorite/quartz diorite, and basalt/andesite (**Figure 2**). Nevertheless, among these rocks, only tonalite and diorite/quartz diorites were examined within the context of this study. Diorites are generally medium grained, hard, black, and less widespread than tonalities, which are medium to coarse grained with intensive alteration resulting in soft topographies. The tonalities contain syn-plutonic mafic dykes and mafic microgranular enclaves of various sizes and shapes, indicating the contemporaneous existence of mafic and felsic magmas [26,27]. Tonalites also contain aplitic dykes. Most of the enclaves found in tonalites are round and elliptical in shape, and their size may reach up to 50 cm. Volcanic rocks in the Keban magmatic province, which covers a large area, are basaltic and andesitic in composition [4], dark in color, fragile, and contain frequent cracks.

Mineralogical studies reveal that Keban magmatics are diorite, quartz diorite, tonalite, and granodiorite in composition. Geochemical data indicate a composition of tonalites, quartz diorites, and diorites. In the geochemical nomenclature diagram [28] (**Figure 3**), two samples are quartz diorite (SK-23 and SK-24), four are diorite (SK-2,-3,-5, and SK-25), and the rest are tonalite in composition.

Medium- to fine-grained diorites and quartz diorites have different granular and poikilitic textures, and are mainly made up of plagioclase and amphibole. In some cases, amphiboles are more dominant than plagioclases. In addition to the main mineral phases, quartz (more dominant in quartz diorite), biotite, pyroxene (as relict), opaque minerals, and secondary minerals such as chlorite, calcite, and epidote are usually observed. Plagioclase generally shows polysynthetic twinning and oscillatory zoning in dioritic rocks. Amphibole generally shows different-sized green pleochroism subhedral and skeletal in structure. The presence of relic pyroxene in some amphibole crystals indicates that these amphiboles are formed by uralitization.

Tonalites and granodiorites are hypidiomorphic, granular textured, and composed of plagioclases, quartz, biotite, amphibole, K-feldspar, zircon, apatite, and opaque minerals (magnetite). Plagioclase, which forms the main felsic mineral, shows albite twinning (An_{15-25}) and zoning. Crystals with overgrowth texture display a sieve texture in some cases. Anhedral quartz varies in size and shows wavy extinction. Minor biotite is generally opacified along the edges, whereas K-feldspar turns to clay. Zircon forms an accessory phase and is generally found with biotite, chlorite, and some quartz, whereas apatite occurs in quartz and plagioclase.

Reaction textures in amphiboles, transformation of amphiboles into biotites, zoning, and sieve textures in plagioclases indicate disequilibrium crystallization in some diorites and tonalites.

The enclaves and syn-plutonic dykes in the tonalities are dark and fine grained. Although the mineralogical composition of these enclaves and the syn-plutonic dykes resembles that of the host-rock, change in the mineral proportions and variation of grain sizes of the plagioclases (seriate texture) are important differences. However, twinning and oscillatory zoning are observed in the plagioclase phenocrysts of these rocks. Such disequilibrium textures observed in phenocrysts are important in determining open system processes such as magma mixing [29].

5. K-Ar HORNBLENDE AGE

K-Ar analysis was conducted on four amphibole separates extracted from fresh rock samples of Keban intrusive rocks. The results are presented in **Table 1**. All four samples (SK-23,-25,-27, and SK-29) solely consist of amphibole grains. Grain size fractions (+212 micron) of the rock samples were extracted. K/Ar ages of 84.8 ± 1.8 and 84.4 ± 1.7 Ma for diorite and quartz diorite samples and 75.7 ± 1.5 and 59.8 ± 1.2 Ma for tonalite samples were obtained. The ages obtained are in accordance with those reported for Baskil granitoids [3,6,30] and Göksun-Afşin granitoids [7,8].

6. GEOCHEMISTRY

6.1. Major and Trace Element Characteristics

Tables 2 and **3** present the results of whole rock chemical analyses of the samples taken from diorites, quartz diorites, and tonalities of the Keban magmatics. Based on the alkali-silica (**Figure 4(a)**), AFM (**Figure 4(b)**) [31], and K_2O-silica [32,33] diagrams (**Figure 4(c)**), the rocks have low-K sub-alkaline characteristics. However, whereas the tonalities show calc-alkaline properties, the diorites and quartz diorites are tholeiitic in character. Examination of the Shand index ($Al_2O_3/(CaO + Na_2O + K_2O)$ versus $Al_2O_3/(Na_2O + K_2O)$ [34] reveals that both diorites and quartz diorites are located in the metaluminous and peraluminous regions (**Figure 4(d)**), whereas the tonalites are located solely in the peraluminous region. The Aluminum Saturation Index (ASI = $Al_2O_3/(CaO +$

Table 1. Data for K-Ar Age determinations in the amphibols of the intruzif rocks.

Sample	Rock	Size (μm)	Age ± 1σ (Ma)	$_{*}{}^{40}$Ar (cc STP/g)	K † (%)	$_{*}{}^{40}$Ar (%)	^{36}Ar (cc STP/g)	$_{*}{}^{40}$K/^{36}Ar	$_{*}{}^{40}$Ar/^{36}Ar
SK-23	Q.diorite	+212	84.76 ± 1.8	6.06E−07	0.18	39.84	3.10E−09	43089	491
SK-25	Diorite	+212	84.35 ± 1.7	5.36E−07	0.16	71.75	7.14E−10	166092	1046
SK-27	Tonalite	+212	75.65 ± 1.5	1.47E−06	0.49	75.70	1.59E−09	227668	1216
SK-29	Tonalite	+212	59.77 ± 1.2	1.60E−06	0.68	80.75	1.29E−09	389714	1534

Table 2. Whole-rock major element (wt%) and trace element (ppm) chemical analysis results of the intruzif rocks.

Sample	Diorite/Quartz diorite						Tonalite										
	SK-2	SK-3	SK-4	SK-5	SK-23	SK-25	SK-1	SK-6	SK-7	SK-8	SK-9	SK-10	SK-11	SK-12	SK-27	SK-28	SK-29
SiO_2	45.33	46.82	47.83	42.28	51.85	47.26	69.91	69.82	72.31	73.12	70.16	69.90	69.97	69.40	71.75	71.81	72.86
Al_2O_3	17.29	19.02	19.50	18.92	18.33	19.64	13.68	14.71	13.75	13.62	15.05	14.77	14.81	14.95	14.03	14.15	13.80
Fe_2O_3	13.06	13.28	11.82	16.77	8.27	9.53	3.76	3.95	3.39	2.39	3.40	3.90	3.95	3.23	3.47	3.45	2.46
MgO	7.30	5.18	5.00	6.53	5.40	6.75	0.98	1.23	1.15	0.47	0.88	1.17	1.13	1.20	0.89	0.92	0.55
CaO	12.23	10.94	11.56	12.43	11.84	13.65	4.33	4.61	4.01	2.71	3.97	4.00	4.27	4.21	3.80	3.87	3.17
Na_2O	2.05	2.33	1.98	1.51	2.01	1.44	4.03	3.81	3.29	4.05	4.10	4.09	4.02	3.93	3.89	3.61	4.02
K_2O	0.15	0.14	0.11	0.08	0.31	0.11	0.50	0.91	1.12	1.61	0.99	0.67	0.23	0.22	0.69	1.19	0.84
TiO_2	0.79	0.82	0.80	1.00	0.49	0.50	0.32	0.41	0.30	0.21	0.30	0.41	0.35	0.34	0.31	0.30	0.22
P_2O_5	0.07	0.11	0.09	0.09	0.04	0.04	0.08	0.10	0.07	0.05	0.07	0.09	0.09	0.09	0.05	0.05	0.03
MnO	0.22	0.22	0.18	0.24	0.15	0.14	0.07	0.10	0.10	0.04	0.11	0.10	0.04	0.05	0.05	0.08	0.03
LOI	1.55	0.94	0.98	0.75	1.4	1.1	2.15	0.69	0.84	1.25	1.15	1.55	1.54	2.11	0.9	0.4	1.8
ASI	0.88	1.04	1.05	0.99	0.95	0.95	1.11	1.13	1.17	1.15	1.19	1.21	1.26	1.30	1.20	1.16	1.23
Total	100.00	99.83	99.85	100.60	100.11	100.18	99.81	100.30	100.30	99.52	100.20	100.60	100.40	99.73	99.86	99.87	99.82
Ni	20	<20	<20	<20	5.9	12.7	<20	<20	<20	<20	<20	<20	<20	<20	10.0	10.2	10.3
Co	37.0	35.0	33.0	52.0	29.0	38.8	5.0	7.0	5.0	3.0	4.0	5.0	5.0	6.0	5.4	5.5	3.3
V	424	351	463	556	221	303	57	71	57	25	41	60	59	54	67	68	47
Cu	20.0	40.0	120.0	120.0	23.5	39.1	10.0	130.0	<10	<10	10.0	<10	<10	<10	3.3	3.9	2.7
Pb	<5	<5	<5	<5	0.3	0.6	<5	5	<5	7	<5	<5	<5	<5	0.6	1.8	1.1
Zn	80	70	70	70	16	9	30	40	50	<30	40	30	<30	<30	12	27	7
Bi	<0.4	<0.4	<0.4	<0.4	<0.1	<0.1	<0.4	1	<0.4	<0.4	<0.4	<0.4	<0.4	<0.4	<0.1	0.1	<0.1
Sn	<1	<1	<1	<1	<1	<1	<1	<1	<1	<1	<1	<1	<1	<1	<1	<1	<1
W	<1	<1	<1	<1	0.9	0.3	<1	<1	<1	<1	<1	<1	<1	<1	2.8	3.3	3.0
Mo	<2	<2	<2	<2	3.5	1.5	<2	<2	<2	<2	<2	<2	<2	<2	15.8	16.8	16.8
As	<5	<5	<5	<5	<0.5	<0.5	<5	<5	<5	<5	<5	<5	<5	<5	<0.5	<0.5	<0.5
Sb	<0.5	<0.5	<0.5	<0.5	<0.1	<0.1	<0.5	<0.5	<0.5	<0.5	<0.5	<0.5	<0.5	<0.5	0.1	0.1	<01
Hg	-	-	-	-	<0.01	<0.01	-	-	-	-	-	-	-	-	<0.01	<0.01	<0.01
Rb	<2	<2	<2	<2	4.0	<0.5	10.0	21.0	25.0	44.0	19.0	9.0	4.0	3.0	20.3	35.5	30.5
Cs	<0.5	<0.5	<0.5	<0.5	<0.1	<0.1	<0.5	<0.5	<0.5	<0.5	<0.5	<0.5	<0.5	<0.5	0.3	0.8	0.5
Ba	26.0	34.0	29.0	18.0	89.9	23.7	120.0	213.0	134.0	255.0	241.0	151.0	90.0	73.0	169.6	174.5	204.5
Sr	182.0	214.0	218.0	204.0	205.7	194.6	186.0	231.0	147.0	152.0	189.0	156.0	266.0	213.0	199.4	214.5	192.7
Tl	<0.1	<0.1	<0.1	<0.1	<0.1	<0.1	<0.1	0.1	0.1	0.2	0.1	<0.1	<0.1	<0.1	<0.1	0.1	<0.1
Ga	16.0	18.0	17.0	19.0	14.4	15.2	12.0	14.0	12.0	12.0	13.0	13.0	13.0	12.0	13.4	13.4	12.4
Ta	<0.1	<0.1	<0.1	<0.1	<0.1	<0.1	0.2	0.2	0.2	0.4	0.2	<0.1	0.2	0.2	0.1	0.2	0.3
Nb	<1	<1	<1	<1	0.8	<0.5	3	3	2	4	2	1	2	2	2.6	3.0	3.8
Hf	0.9	1.0	0.8	0.8	1.0	0.8	3.0	3.4	2.5	2.9	2.4	6.0	3.0	3.0	3.1	3.2	3.0
Zr	23.0	23.0	21.0	17.0	30.4	15.6	109.0	143.0	90.0	104.0	86.0	226.0	110.0	101.0	101.7	119.0	96.4
Y	18.0	28.0	18.0	21.0	13.7	13.3	17.0	17.0	17.0	11.0	15.0	21.0	16.0	17.0	17.2	15.1	15.2
Th	0.2	0.6	0.2	<0.1	0.7	<0.1	2.0	2.7	2.2	6.3	2.4	1.0	1.8	2.0	2.5	2.3	5.2
U	0.2	0.2	0.1	0.2	0.4	<0.1	0.9	0.8	1.1	1.9	1.1	0.5	0.8	0.9	1.1	0.9	1.4
Rb/Sr	0.01	0.01	0.01	0.01	0.02	0.00	0.05	0.09	0.17	0.29	0.10	0.06	0.02	0.01	0.01	0.17	0.16
K_2O/ P_2O_5	2.14	1.27	1.22	0.89	7.75	2.75	6.25	9.1	16.0	32.2	14.14	9.57	2.55	2.44	14.0	24.0	28.0
Ba/Nb	28.9	37.8	32.2	20.0	112.37	51.52	40.0	71.0	67.0	63.7	120.5	151.0	45.0	36.5	62.23	58.17	53.81
La/Nb	14.0	34.0	25.0	13.0	2.8	2.8	2.7	3.0	3.9	3.6	3.8	5.9	3.5	3.1	2.6	2.6	3.0
Zr/Nb	28.7	28.7	23.3	18.9	38.0	39.0	36.3	47.7	45.0	26.0	43.0	226.0	55.0	50.5	39.1	39.7	25.4
Nb/U	4.5	3.0	4.5	3.0	2.0	4.4	3.3	3.8	1.8	2.1	1.8	2.0	2.5	2.3	2.4	3.3	2.7

Table 3. Whole-rock REE element (ppm) chemical analysis results of the intruzif rocks.

Sample	Diorite/Quartz diorite						Tonalite										
	SK-2	SK-3	SK-4	SK-5	SK-23	SK-25	SK-1	SK-6	SK-7	SK-8	SK-9	SK-10	SK-11	SK-12	SK-27	SK-28	SK-29
La	1.4	3.4	2.5	1.3	2.2	1.3	8.1	9.0	7.8	14.4	7.5	5.9	6.9	6.2	6.8	7.9	11.3
Ce	4.5	8.8	5.9	4.3	5.6	3.8	15.9	17.1	14.6	24.9	14.2	13.6	14.0	12.5	14.6	15.8	21.5
Pr	0.92	1.57	1.00	0.94	0.84	0.65	2.12	2.21	1.94	2.83	1.81	2.04	1.92	1.76	1.77	1.84	2.34
Nd	5.7	8.9	5.5	5.9	4.7	3.2	8.5	8.9	7.6	9.6	7.1	9.4	7.8	7.5	7.3	7.6	9.0
Sm	2.1	3.0	1.8	2.2	1.4	1.2	2.2	2.3	2.0	2.0	1.9	2.6	2.0	2.1	1.9	1.7	1.7
Eu	0.85	0.93	0.72	0.90	0.57	0.46	0.65	0.77	0.61	0.49	0.68	0.78	0.68	0.69	0.59	0.62	0.53
Gd	3.0	4.3	2.8	3.3	1.72	1.61	2.6	2.8	2.6	1.9	2.3	3.2	2.5	2.5	2.03	1.89	1.72
Tb	0.6	0.8	0.5	0.6	0.37	0.33	0.5	0.5	0.5	0.3	0.4	0.6	0.5	0.5	0.43	0.38	0.32
Dy	3.5	5.0	3.3	3.9	2.23	2.12	2.8	3.0	2.9	1.9	2.5	3.6	2.8	2.9	2.49	2.26	1.82
Ho	0.7	1.1	0.7	0.8	0.47	0.52	0.6	0.6	0.6	0.4	0.5	0.8	0.6	0.6	0.57	0.51	0.46
Er	2.2	3.1	2.0	2.4	1.45	1.38	1.9	2.0	2.0	1.3	1.7	2.5	1.9	2.0	1.83	1.49	1.43
Tm	0.34	0.48	0.30	0.37	0.20	0.20	0.32	0.33	0.35	0.23	0.29	0.43	0.31	0.32	0.29	0.24	0.25
Yb	2.2	3.1	1.9	2.4	1.35	1.41	2.2	2.2	2.4	1.7	2.0	3.2	2.2	2.3	1.81	1.60	1.63
Lu	0.35	0.46	0.28	0.35	0.23	0.22	0.37	0.36	0.36	0.30	0.32	0.54	0.35	0.39	0.31	0.26	0.28
La/Yb_{CN}	0.46	0.79	0.94	0.39	1.17	0.66	2.64	2.93	2.33	6.08	2.69	1.32	2.25	1.93	2.69	3.54	4.97
Eu/Eu*	1.03	0.79	0.98	1.02	1.12	1.01	0.83	0.93	0.82	0.77	0.99	0.83	0.93	0.92	0.92	1.06	0.95

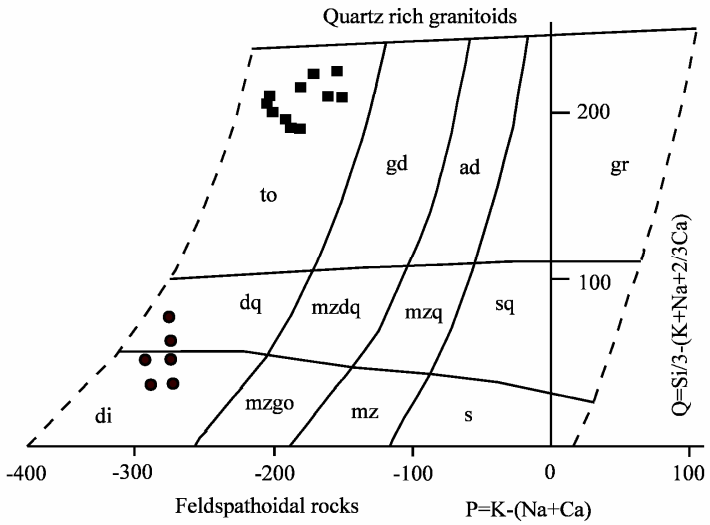

Figure 3. Nomenclature diagram for the Keban magmatic rocks [28]. di: Diorite, dq: Qurtz diorite, to: Tonalite.

Na_2O + K_2O)) [35] values are greater than 1 (**Figure 4(d)**), which is in accordance with mafic mineral association, such as biotit + amphibol. Zr, Nb, and Y-SiO_2 (**Figures 4(e)-(g)**) diagrams indicate that these rocks have I-type granitoid character.

Compositional differences in these rocks are also observed in the main and trace elements versus silica diagrams. These units undergo different fractional crystallization processes (**Figure 5**). Diorites have higher Al_2O_3 than tonalites (**Figure 5(a)**), indicating that the fractionation process is effective in differentiation. Depending on the mafic phase composition, CaO, FeO, MgO, MnO, and Ti_2O are higher in diorites than tonalites (**Figures 5(b)-(f)**). However, tonalites have richer con- tent of main oxides, such as K_2O and Na_2O, depending on feldspars rich in K and Na (**Figures 5(g)** and **(h)**). The same degree of P_2O_5 enrichment (**Figure 5(i)**) in both rock groups indicates the presence of apatite in the rocks. The negative correlation of the main elements, such as Al_2O_3, CaO, FeO*, MgO, MnO, and Ti_2O, with SiO_2 and its

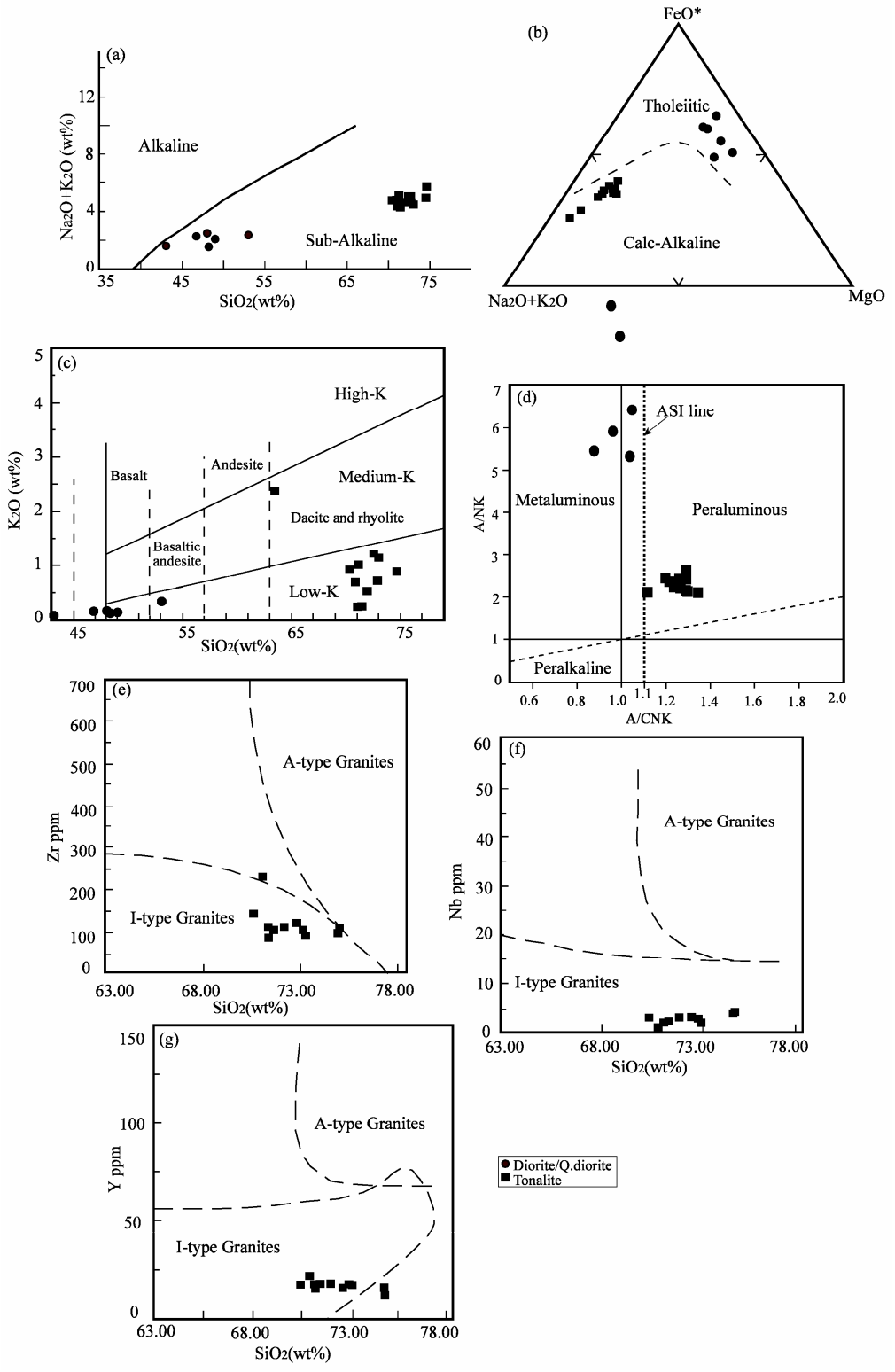

Figure 4. Major element geochemical discrimination diagrams of the Keban magmatic rocks. (a) Total alkalis vs silica ([31], dividing line between alkaline and sub-alkaline fields [32]); (b) AFM triangular diagram [31]; (c) K_2O vs silica [33]; (d) Shand Index ([34], ASI: Aluminum Saturation Index = molar Al_2O_3/molar (CAO + Na_2O + K_2O [35]) and (e-g) Plot of thr Keban magatic rocks on the I/A-type granites diagram [36]).

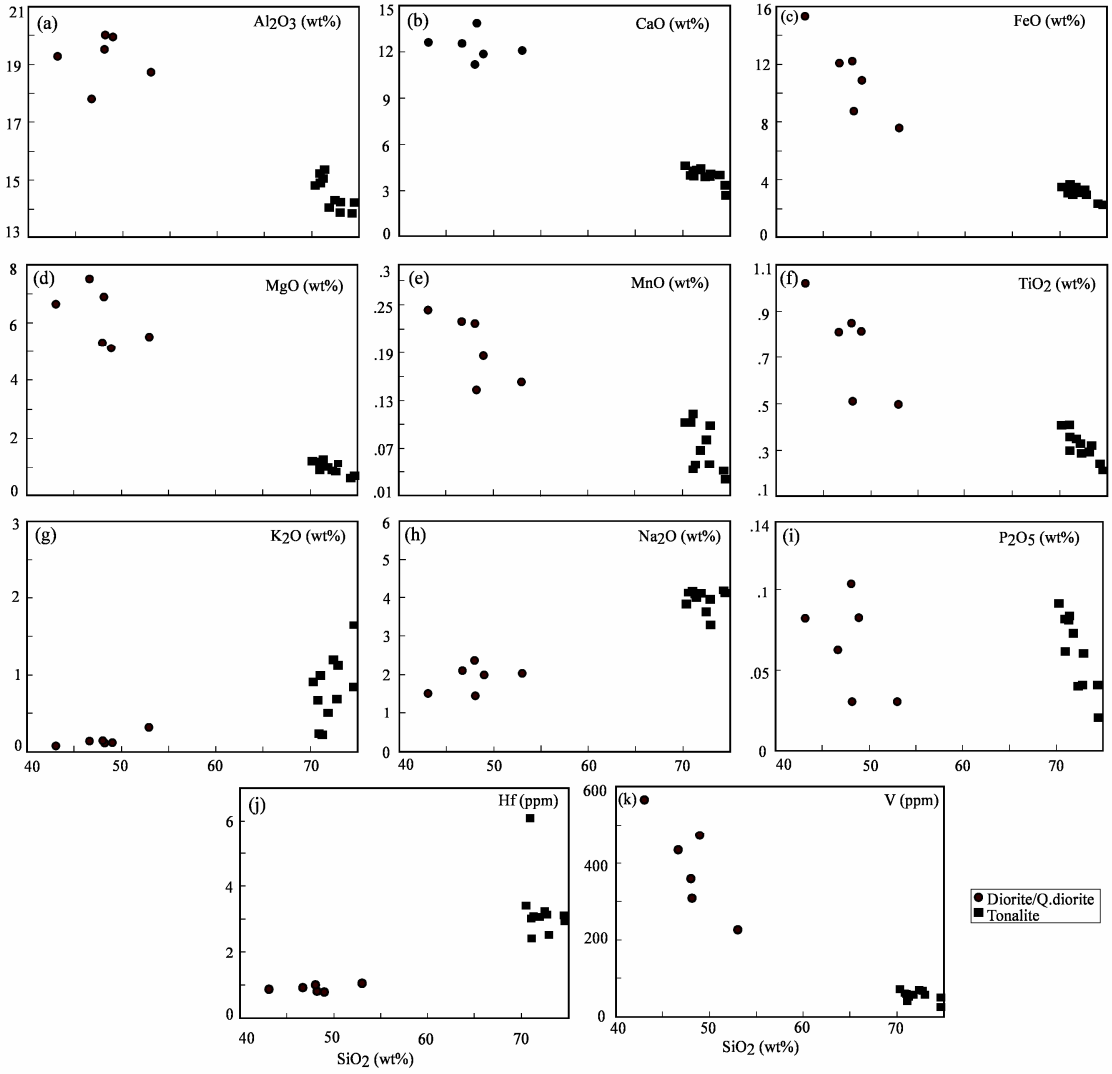

Figure 5. Magor oxides and some trace elements vs. SiO_2 variation diagrams for rocks samples from the Keban magmatic rocks.

positive correlation with Na_2O and K_2O in both rock groups indicate fractional crystallization during magma evolution. The variations of the trace elements, Hf and V, with SiO_2 (**Figures 5(j)** and **(k)**) are further indications of fractional crystallization. Fractionation phases are mainly plagioclase, pyroxene, and hornblende.

The chondrite-normalized spider diagram (**Figure 6(a)**) demonstrates the differences between the tonalites and diorites in terms of LREE. In general, tonalites show higher LREE [$(La/Yb)_{CN}$ = 6.08 – 1.32], whereas diorites are more depleted in these elements [$(La/Yb)_{CN}$ = 1.17 – 0.39]. Except for the negative Eu anomaly (Eu/Eu* = 0.79) in Sample SK-3, the other samples from the diorites do not show negative Eu anomalies (Eu/Eu* = 1.12 – 0.98). All samples of the tonalites display negative Eu anomalies (Eu/Eu* = 0.99 – 0.77) except sample SK-28 (Eu/Eu* = 1.06). In addition, the upward concave distribution from LREEs to HREEs, especially in the tonalities, emphasizes the importance of the feldspars in tonalites during fractionation and melting [37].

In the MORB-normalized spider diagrams, tonalites are richer in LREE, similar to previous diagram (**Figures 6(b)** and **(c)**). However, the distributions of some elements remarkably vary in tonalites and diorites. For instance, whereas Hf and Zr are depleted to the extent of negative anomaly in diorites, these elements are enriched in tonalites.

Crustal-origin elements, such as K, Rb, Ba, Th, and Y, are found with fewer amounts in diorites than in tonalities. Ti, which represents the mantle, shows remarkable negative anomaly. These findings confirm that these elements are compatible with each other. Although such

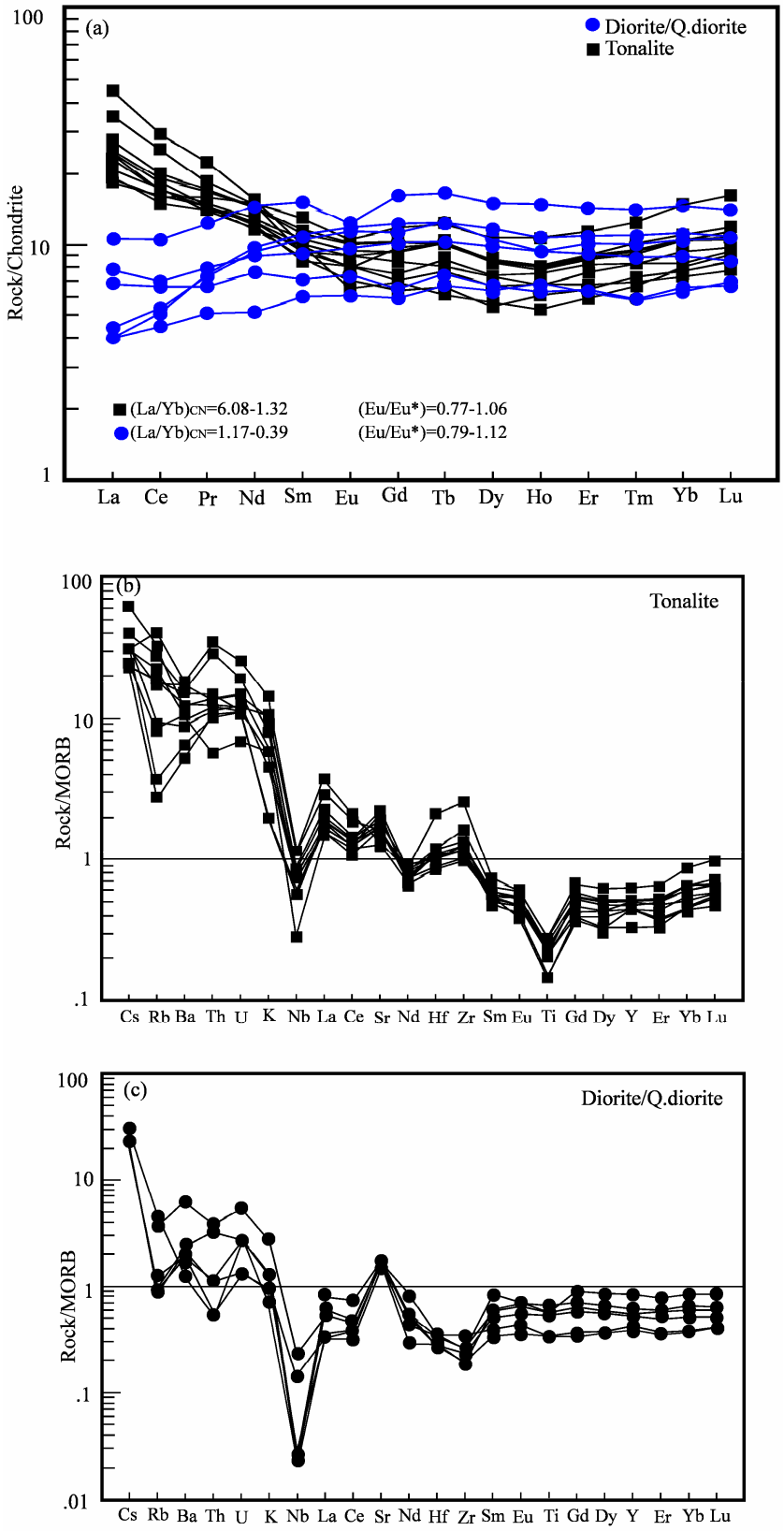

Figure 6. Chondrite (a) and MORB (b-c) normalized spider diagrams for the Keban magmatic rocks. MORB and Chondrite-normalizing values [38].

distribution coincides with the mature period of arc plutonism [39], acidic magma can be said to have formed as a result of the contamination of magma with basic-intermediate composition or its assimilation. The HREE between Gd-Lu is more enriched in tonalites.

6.2. Sr and Pb Isotope Geochemistry

The Pb and Sr isotope ratios of the samples are presented in **Table 4**. Sr isotope ratios in diorites are SK-23 = 0.704828 and SK-25 = 0.704754. They are higher in tonalities, with SK-27 = 0.705405 and SK-29 = 0.706053. The Pb isotope ratios display similar distribution in tonalites and diorites (**Table 4**).

The distributions of the samples were analyzed in different isotope variation diagrams (**Figure 7**). According to these analyses, the samples in the $^{87}Sr/^{86}Sr$ - $^{206}Pb/^{204}Pb$ diagram are positioned close to the Upper Continental Crust and Lower Continental Crust (**Figure 7(a)**) but are mainly found in the Ocean Island Basalt (OIB) zone. Three samples in the $^{208}Pb/^{204}Pb$ - $^{206}Pb/^{204}Pb$ diagram are found in Enriched Mantle II (EM II), and one sample from the acidic rocks is in the enriched oceanic sedimentary zone very close to the EM II zone (**Figure 7(b)**). Such distribution indicates that the samples have compositions similar to those of enriched mantle sources and that the differentiation between I-type granitoids and crustal materials plays an active role in the formation of the magma. The intensification of samples in the $^{207}Pb/^{204}Pb$ - $^{206}Pb/^{204}Pb$ diagram (**Figure 7(c)**) around the EM II or pelagic sediment zone may indicate the presence of a sedimentary rock in the mantle source or the contamination of large magma masses resulting from a used-up under-continent lithospheric mantle. However, the greater concentration in our samples around EM II can be better interpreted as the presence of continental crust traces in the source rock or the presence of continent-derived sediments [40,41].

7. DISCUSSIONS

Based on the evaluation of mineralogical-petrographic and geochemical studies (**Figures 3-6**), these intrusive rocks indicate two different phases with I-type granitoid property. Thus, utilizing these data is important to determine the crystallization processes [*i.e.*, fractional crystallization (FC) and accumulation fractional crystallization (AFC)] of the magma forming the Keban magmatics, magma mixing, and source characteristics. These issues will be discussed within this context.

7.1. Interpretation of Amphibole K-Ar Ages

Two amphibole separates extracted from diorites and quartz diorites yielded similar K-Ar ages of about 85 Ma (**Table 1**). This finding indicates synchronous cooling below 500˚C based on the blocking temperature of radiogenic Ar in amphibole minerals [42]. The two amphibole ages from the tonalites are not consistent with each other (**Table 1**). Samples SK-27 and SK-29 yielded ages of about 75 and 60 Ma, respectively. This age difference may have resulted from amphibole minerals, which were crystallized at different stages during the solidification of magma; *i.e.*, the older K-Ar age data may come from early-stage amphibole minerals first crystallized during FC. Another reason could be the loss of radiogenic Ar, which could result in low K-Ar age of the rock sample SK-29. This sample shows an alteration effect under microscopy, *i.e.*, chloritization and epidotization of biotites, sericitization and saussuritization of feldspars, and opacitizations of amphibole minerals. In this circumstance, an age interval between approximately 85 and 60 Ma is suggested as the most reliable amphibole K-Ar cooling age for Keban magmatics.

7.2. Crystallization Processes

The main processes of magma crystallization in Keban magmatics are FC, magma mixing, and AFC. Based on the Rock/Chondrite diagram (**Figure 6(a)**), FC is developed as the FC of different magmatic phases in acidic and intermediate magmas.

The negative correlation of CaO, FeO*, MgO, MnO, TiO_2, and P_2O_5 composition with increasing silica and its positive correlation with Na_2O and K_2O in the Harker diagrams (**Figure 5**) indicate the FC effect, especially in basic/intermediate rocks. The 5.00 - 7.30 variation of the MgO content in diorite and quartz diorites further indicates the predominance of olivine and pyroxene in fractionation phase. This variation is also observed in the

Table 4. Sr and Pb isotope geochemical data.

Sample	Rock	Sr (ppm)	Rb (ppm)	$^{87}Rb/^{86}Sr$	$(^{87}Sr/^{86}Sr)_0$	$(^{87}Sr/^{86}Sr)i$	$^{206}Pb/^{204}Pb$	$^{207}Pb/^{204}Pb$	$^{208}Pb/^{204}Pb$
SK-23	Q diorite	205.7	4.0	0.0562	0.704828	0.70476	19.0597	15.6553	38.8229
SK-25	Diorite	194.6	0.5	0.0074	0.704754	0.70475	18.5931	15.6144	38.4978
SK-27	Tonalite	199.4	20.3	0.2945	0.705405	0.70509	18.9903	15.6472	38.8670
SK-29	Tonalite	192.7	30.5	0.4579	0.706053	0.70566	19.0272	15.6678	38.9609

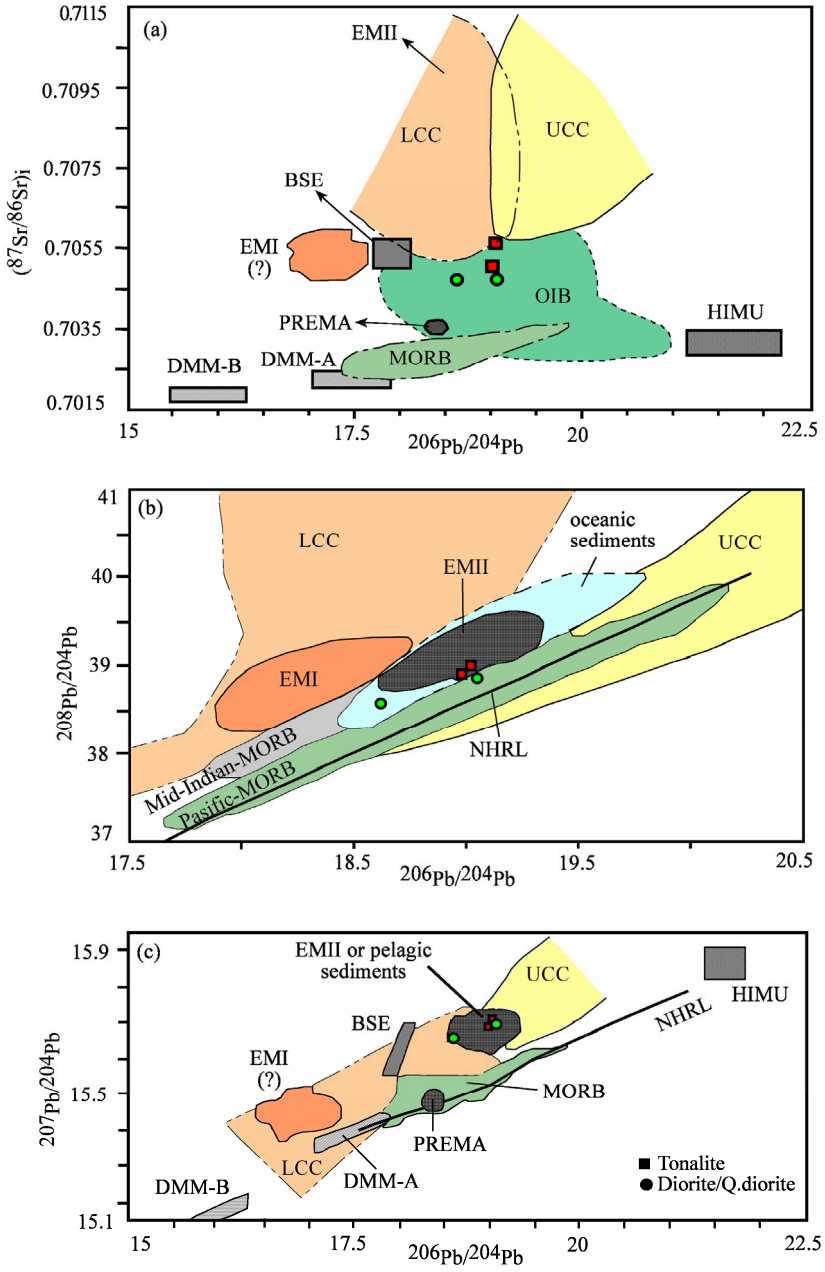

Figure 7. (a) 206Pb/204Pb vs. $(87Sr/86Sr)_i$, (b) 206Pb/204Pb vs. 208Pb/204Pb and (c) 206Pb/204Pb vs. 207Pb/204Pb variation diagrams of the rock samples from the Keban magmatic rocks [40]. OIB (Oceanic Island Basalts), UCC (Upper Continental Crust), LCC (Lower Continental Crust), NHRL (Northern Hemisphere Reference Line), HIMU (mantle with High U/Pb ratio), PREMA (frequently observed PREvalent Mantle composition), BSE (Bulk Silicate Earth), EMI and EMII (Enriched Mantle), DMM (Depleted Mantle).

change in LILE and HFSEs with silica, enabling the formation of some major rock-forming minerals (**Figure 8**). The increase in Rb content caused by the silica diagram in diorite and quartz diorites (**Figure 8(a)**) indicates AFC processes, whereas Ba and Sr-SiO_2 variation diagrams signify pyroxene (orthopyroxene and clinopyroxene) fractionation for these rocks (**Figures 8(b)** and **(c)**). There is no evident trend in tonalites in Rb and Ba compositions, and biotite and K-feldspar fractionation is an observed trend in Sr (**Figure 8(c)**). The Y-silica variation diagram shows the effect of amphibole in diorites and tonalites (**Figure 8(d)**). The effect of amphibole on the

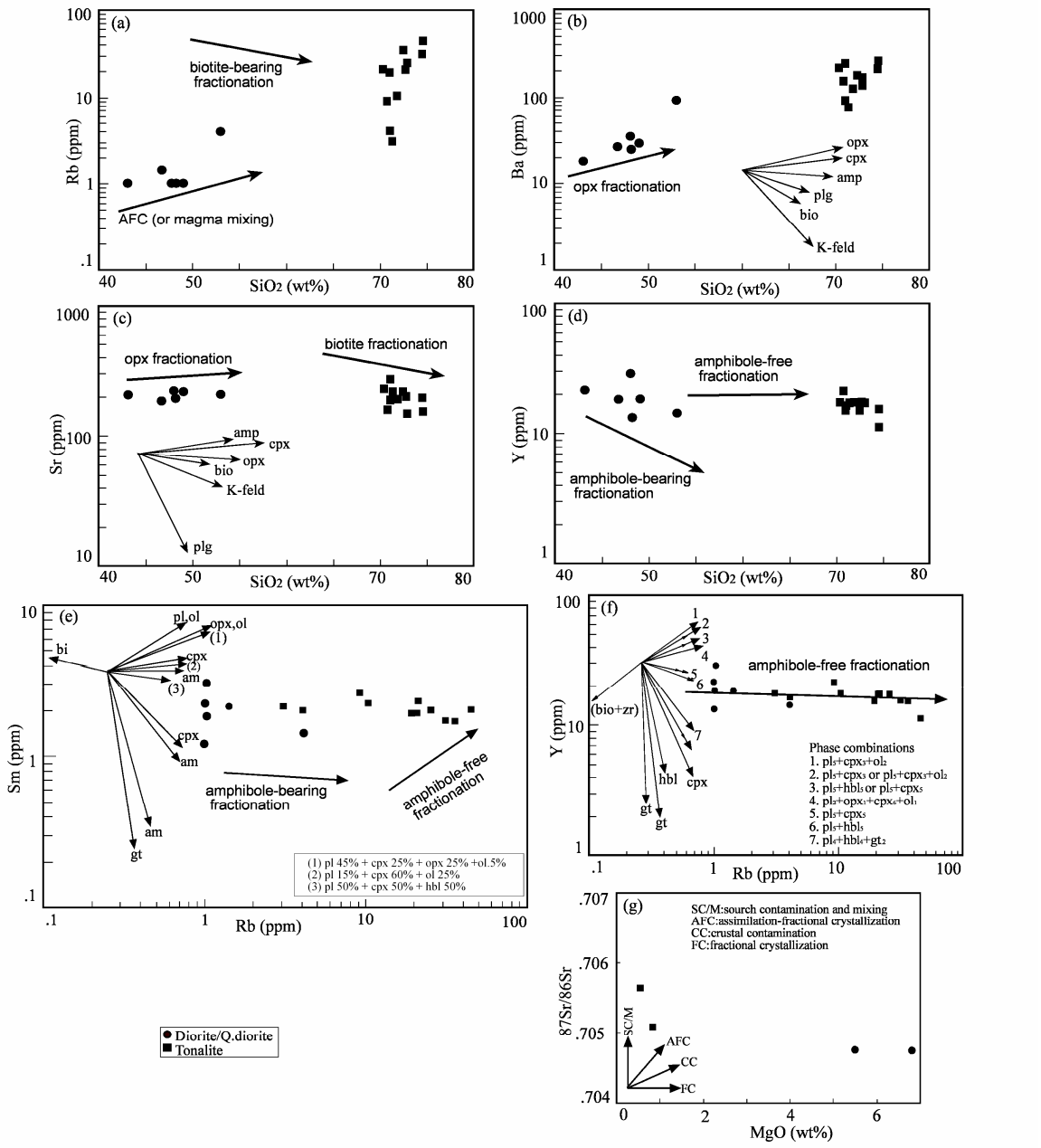

Fiure 8. Rb, Ba, Sr and Y vs. silica (a-d) semi-logarithmic variation diagrams of various I-type granites from the Keban magmatic rocks, Arrows were taken after [43], and they indicate theoretical Rayleigh fractionation vectors modelled for crystallization of indicidual mineral phases. Theoretical vectors for the likely crystallizing phases are for 50% fractionation of single phases. Partition coeddicients used for the modelling are from the compilation [37]. (e) Sm vs Rb variation diagram [44]. (f) Y vs Rb variation diagram [45]. (g) MgO-87Sr/86Sr cariation diagram. Opx, orthopyroxene; cpx, clinopyroxene; amp, amphibole; plg, plagioclase; bio, biotite; K-feld, K-feldspar; hb,hornblende; gt, garnet; zr, zircon; ol, olivine.

crystallization process of the tonalites is also visible in Sm-Rb and Y-Rb variation diagrams (**Figures 8(e)** and **(f)**). A weak effect of amphibole on diorites is also observed. Different from the above-mentioned diagrams, the $^{87}Sr/^{86}Sr$-MgO variation diagram demonstrates the effect of FC on diorites and the effect of source contamination/mixing (SC/M) on tonalites (**Figure 8(g)**).

In addition to all these data, the ratios among the highly incompatible elements are used in petrogenetic processes, such as partial melting and fractional crystallization. For example, Zr/Y is not greatly affected by fractional crystallization in basaltic system, but it changes

during partial melting [46]. In case of a low melting degree, the Zr/Y rate is high. This finding corresponds to the changed rate of Y, which is higher than Zr. Accordingly, Zr/Y rates in the samples (**Figure 9)** markedly show that the partial melting processes changed during the formation of rocks. This change can be clearly observed between tonalites and diorites. Tonalites are also influenced by different melting degrees. Rocks have different Fe contents, depending on the differences in their mantle source compositions. As a result, high Fe content and Zr/Y rate indicate high pressure or low melting rates during magma formation processes.

Aside from the field data on the presence of MME and syn-plutonic dykes in Keban magmatics, the existence of special textural properties, such as skeleton structure in the minerals, oscillator zoning, and acicular apatites, indicates the mixing of mantle and crustal magma [47]. This interaction between acidic and intermediate-composition rocks emerges from the different distributions of the elements in the geochemical data (**Figures 8(a)-(g)**). In these data, AFC processes were observed in both rock groups. Therefore, the co-development of crust assimilation and FC is more effective in the crystallization of the felsic magma.

7.3. Source Characteristics

Ni content is an important indicator of whether the source material in the plutonic rocks is primitive or depleted mantle. Low Ni content (5.9 - 19 ppm) in Keban magmatics demonstrates that the source material is not primitive mantle but depleted mantle melt that underwent significant fractional crystallization [48]. The diorites seem entirely derived from the mantle in the Na_2O-K_2O diagram (**Figure 10(a)**), whereas it is generally concentrated in the region of depleted mantle in the Zr/Yb-Nb/Yb diagram (**Figure 10(b)**). The diorites also demonstrate a passage to the E-MORB. The same diagram demonstrates that the tonalites are concentrated in the E-MORB region, whereas the Sm/Yb-Ce/Sm diagram (**Figure 10(c)**) shows that the diorites are in MORB, and the tonalites are in the interaction site of MORB-OIB. This kind of concentration can be created by subduction zone enrichment or crust contamination [53].

Crustal interaction is evident in the Rb/Y-Nb/Y and Ba/La-Ce/Pb diagrams (**Figures 10(d)** and **(e)**). Furthermore, the effect of subduction is apparent in the Th/Yb-Ta/Yb (**Figure 10(f)**) diagram used in magmatic petrology [53]. The FC effect is also visible in this diagram.

Although Keban magmatics generally display MORB property in the diagrams (**Figures 10(a)-(f)**), they also show eastern Hebei granulites, compositional property of arc volcanites, and classic continental sedimentary in the

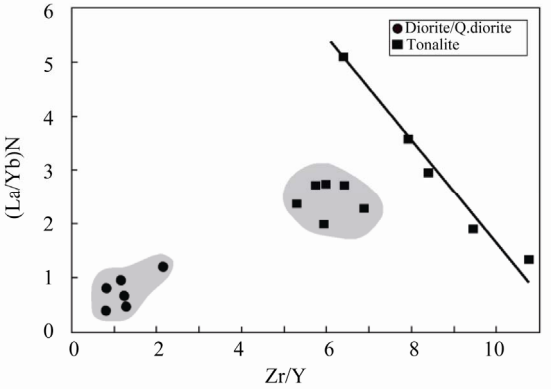

Figure 9. Distribution of the Zr/Y-(La/Yb)N diagram for the Keban magmatic rocks. Normalizing values [38].

Ba/Nb-La/Nb diagram (**Figure 10(g)**). This effect is due to enrichment of the mantle material by the upper crust sediments before partial melting.

As previously mentioned, a clear indicator of the effectiveness of crustal contamination is the increase in Rb/Sr and K_2O/P_2O_5 depending on SiO_2 (**Table 2**) [55]. However, this indicator should be considered together with AFC and partial melting [56].

The high values of some element ratios, such as Ba/Nb (diorite = 20 - 112; tonalite = 40 - 151) and Zr/Nb (diorite = 19 - 39; tonalite = 26 - 226; **Table 2**), in Keban magmatics, which are observed to have similar compositional properties with the mantle wedges in some of the diagrams presented, denote that these rocks were subjected to mantle-derived depletion [57]. The La/Nb ratios used to differentiate between asthenospheric and lithospheric mantle sources are higher than 1 (La/Nb > 1) in sub-continental lithospheric mantle sources and lower than 1 (La/Nb < 1) in asthenospheric mantle sources. La/Nb value > 1 in all the samples (1.4 - 5.9) is another indicator of the lithospheric mantle property of these rocks [58]. However, some researchers suggest that relative depletion, especially in Nb and Ta, could be caused by the interaction between the sub-continental lithospheric mantle and the asthenospheric melt [59].

Similarly, frequent modification of sub-continental lithospheric mantle caused by dehydration in the subduction zone and its sediment content [38] causes relative depletion of Ti, Nb, and Ta and the enrichment of Ba. The remarkably negative anomaly of Nb and Ti in Keban pluton diorites and tonalites indicates that apatite and Fe-Ti oxides play an important petro-genetic role in the formation of rocks [60].

These data on magma origin show that Keban magmatics were formed from a single source. However, in this petro-genetic process, the two rock groups were developed by FC, AFC, and magma composition processes. Accordingly, they were formed in two different phases.

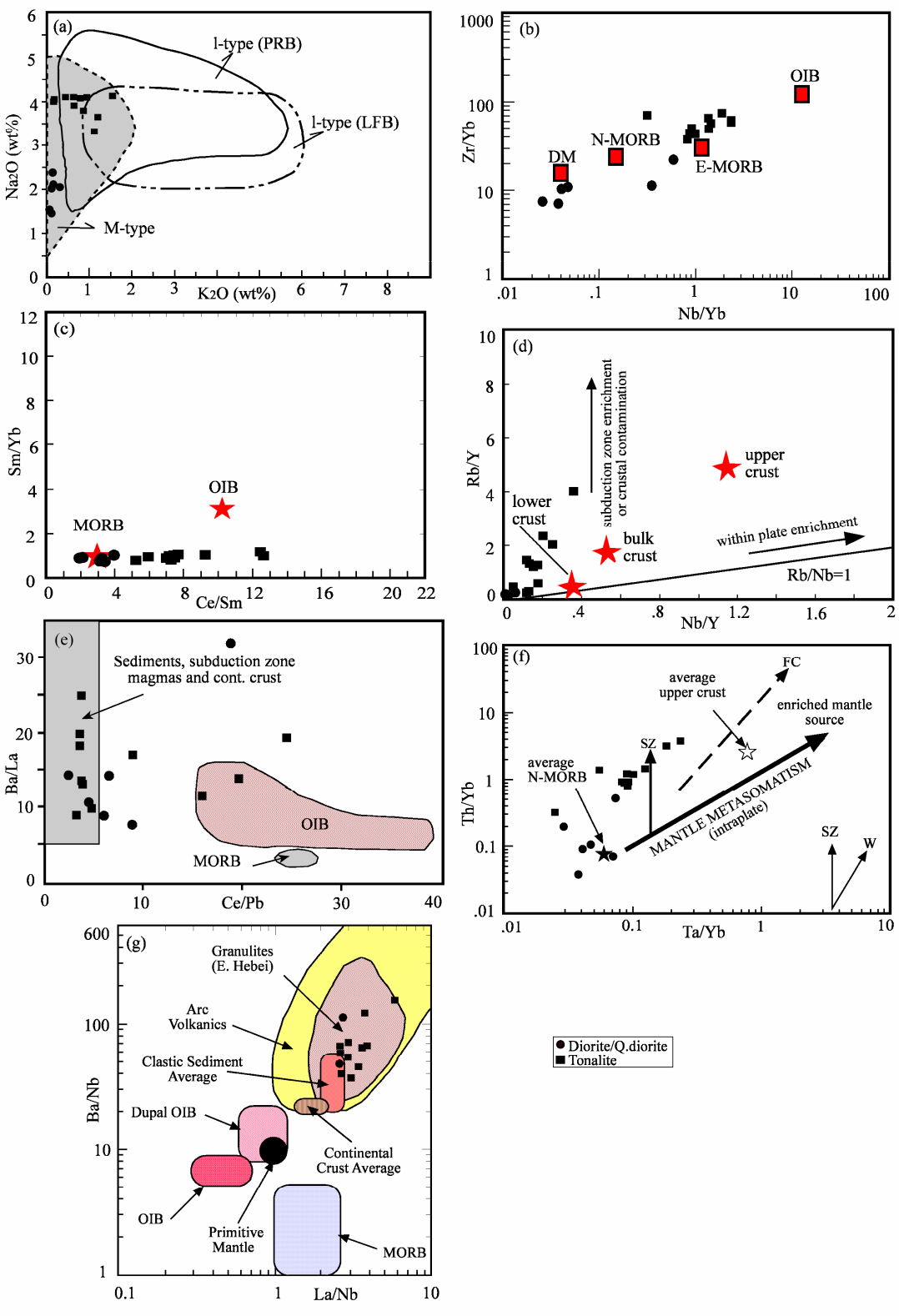

Figure 10. (a) Na_2O vs K_2O, PRB: batolites of the arc-magmatism in the subduction zones. PFB: lower crust of fractional—crystallization granitoides. M-type: subfield derived-mantle granitodes [49]. (b) Zr/Yb vs Nb/Yb and (c) Sm/Yb vs. Ce/Sm [50]; (d) Rb/Y VS Nb/Y [51]; (e) Ba/La vs Ce/Pb [52]; (f) Th/Yb vs. Ta/Yb; (g) Ba/Nb vs. La/Nb plots of the rock samples from the Keban magmatic rocks.

Crustal interaction and hybrid magma textures in tonalites are indicative of this.

In the samples, $^{87}Sr/^{86}Sr$ in diorites/quartz diorites is 0.704, which shows that this magma formed from an isotopically derived lithospheric mantle. The tonalites, with values of $^{87}Sr/^{86}Sr$ = 0.705 - 0.706, are derived from the mixing of the upper mantle material of the same properties. Typical mafic and magma originated from the lower crust.

7.4. Geodynamic Interpretation

In many studies conducted in the region, various tectonic models have been suggested for the tectonomagmatic units in southeast Anatolia. One premise is that the Neotethyan oceanic was closed in the late Cretaceous era [24]. However, in this model, the existence of the platform carbonates (Malatya-Keban) and arc-type intrusive rocks such as Baskil granitoids is difficult to explain [7]. Another suggestion is that southern Neotethyan was closed in middle Miocene [61]. Some authors suggest that the closing of the southern Neotethyan was completed with the emplacement of ophiolites in late Cretaceous [7,62-65]. Despite these controversies related to the closure of the Tethyan oceanic basin and its relevant formations, the tectonomagmatic/stratigraphic units in the southeast Anatolia orogenic system are undisputable: metamorphic massifs (Malatya-Keban platform carbonates), SSZ ophiolites (Göksun, İspendere, Kömürhan, Guleman), ophiolite-related metamorphic rocks (Berit metaophiolite), and granitoides (Göksun, Doğanşehir, Baskil). All granitoids in this belt are intruded into metamorphosed platform carbonates and ophiolites.

Keban magmatics, which have volcanic-arc magmatics characteristics (**Figure 11**), are in harmony with all these granitoids in terms of petrographic, chemical, and radiogenic isotope ages and geologic positioning. Therefore, in the regional scale, they must be discussed within the context of the Malatya-Keban platform and Baskil arc magmatics.

8. CONCLUSIONS

Keban magmatics, which widely crop out between Elazığ and Keban, represent two different phases in the composition of diorites/quartz diorites and tonalites. The two units show subduction zone VAG and I-type granitoid properties as well as different K-Ar amphibole ages of 84 - 85 Ma in diorites/quartz diorites and 60 - 75 Ma in tonalites. According to the age data on Keban magmatics, rocks with acidic composition have been intruded later than the basic ones. These results are in accordance with the field data.

Major and trace element variations indicate the effect

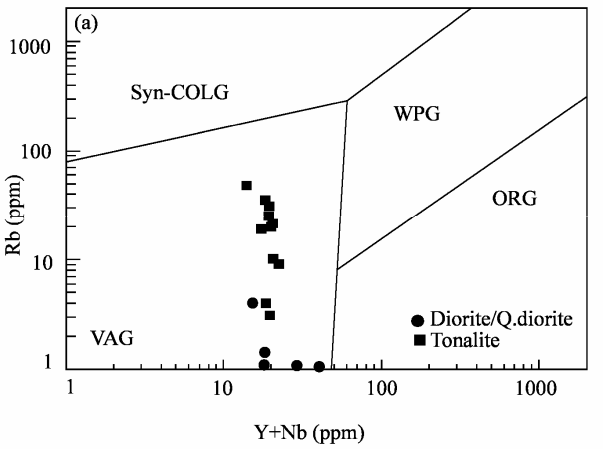

Figure 11. Rb (ppm) vs Y + Nb (ppm) geotectonic discrimination diagrams for the Keban magmatic rochs. Syn-COLG, syn-collisional granitoids; WPG, within-plate garnitoids; VAG, volcanic-arc granitoids; ORG, ocean-ridge granitoids.

of mineral fractionation during the formation of both rock groups, especially fractionation of plagioclase, hornblende, pyroxene, and olivine, aside from apatite and Fe-Ti oxides.

The enrichment in LIL elements, as observed in the tonalities, can be explained by the enrichment of mantle-derived magmas by crustal contamination [66]. Very strong negative anomalies of Ti and Nb in tonalites are apparent, whereas those in diorites only deplete Nb. This feature confirms that aside from the similarity with the subduction zone series, diorites may also be mantle derived.

In light of all the data, this pluton can be inferred to be composed of diorites, which developed in the pre-collision environment. These plutons are formed by a mantle-derived mafic magma source and tonalites derived from the mantle and crust developed in the post-collision environment. The tonalites are affected by the mafic and felsic magma mixture formed by the magma melting the crust during its injection into the crust or its ascent through the crust.

The frequent modification of the sub-continental lithospheric mantle caused by dehydration in the subduction zone and the subduction sediments causes a proportional depletion in Ti, Nb, and Ta and enrichment in Ba. The strongly negative anomalies of Nb and Ti in diorites and tonalites in the Keban pluton can be considered indicators of subduction sediments, as observed in the diagrams. The negative Ti anomaly indicates that apatite and Fe-Ti oxides petrogenetically play an important role in the generation of this magma.

According to the petrographic, geochemical, and radiogenic isotope data, Keban magmatics have petrographic, geochemical, geochronologic, and geotectonic

characteristics similar to Göksun-Afşin, DoğanşehirPolat-Begre, and Baskil-Pertek granitoids located in the Southeast Anatolia orogene region [1-8].

9. ACKNOWLEDGEMENTS

I am indebted to Prof. Durmuş Boztuğ, Dr. Orhan Karsli and Dr. Erhan Akay for reading and correcting the manuscript.

REFERENCES

[1] Aktaş, G. and Robertson, H.F. (1984) The maden complex, S E Turkey: Evolution of a neotethyan active margin: The geological evolution of the Eastern Mediterranean. In: Dixon, J.E and Robertson, A.H.F., Eds. *Geology Society of London Special Publication*, **17**, 372-402.

[2] Asutay, H.J. (1988) Baskil (Elazığ) çevresinin jeolojik ve petrografik incelenmesi. MTA Dergisi, 107.

[3] Yazgan, E. and Chessex, R. (1991) Geology and tectonic evolution of the south-eastern Taurides in the region of Malatya. *Turkish Petroleum Geologists Bulletin*, **3**, 1-42.

[4] Akgül, B. and Bingöl, A.F. (1997) The magmatic rocks of the petrographic and petrologic features in the area of Piran (Keban). Selçuk Üniversitesi Mühendislik Mimarlık Fakültesi 20, Yil Jeoloji Sempozyumu, 13-24.

[5] Rızaoğlu, T., Parlak, O., Koller, F., Höck, V. and İşler, F. (2005) Geochemistry and tectonic significance of the Baskil granitoid rocks from the Southeast Anatolian Orogen (Elazığ, Turkey). *International Symposium on the Geodynamics of Eastern Mediterranean*: *Active Tectonics of the Aegean Region*. Kadir Has University, İstanbul, 228.

[6] Rızaoğlu, T., Parlak, O., Höck, V., Koller, F., Hames, W.E. and Billor, Z. (2009) Andean-type active margin formation in the eastern Taurides: Geochemical and geochronogical evidence from the Baskil granitoid (Elazığ, SE Turkey). *Tectonophysics*, **473**, 188-207.

[7] Parlak, O. (2006) Geodynamic significance of granitoid magmatism in the southeast Anatolian orogen: Geochemical and geochronolgical evidence from Göksun-Afşin (Kahramanmaraş, Turkey) region. *International Journal of Earth Sciences* (*Geol Rundsch*), **95**, 609-627. doi:10.1007/s00531-005-0058-2

[8] Parlak, O., Rızaoğlu, T., Bağcı, U., Karaoğlan, F. and Höck, V. (2009) Tectonic significance of the geochemistry and petrology of ophiolites in southeast Anatolia, Turkey. *Tectonophysics*, **473**, 173-187. doi:10.1016/j.tecto.2008.08.002

[9] MTA. (2002) 1/500.000 Turkiye jeoloji haritasi. General Directorate of Mineral Research and Exploration, Ankara.

[10] Rızaoğlu, T., Parlak, O., Höck, V. and İşler, F. (2006) Nature and significance of late cretaceous ophiolitic rocks and its relation to the Baskil granitoid in Elazığ region, SE Turkey. *Geological Society*, Special Publication, **260**, 327-350.

[11] Tarhan, N. (1986) Doğu toroslarda neo-tetis'in kapanımına ilişkin granitoyid magmalarının evrimi ve kökeni. *M.T.A. Dergisi*, **107**, 95-110.

[12] Yılmaz, Y. (1993) New evidence and model on the evolution of the Southeast Anatolian orogen. *Geological Society of America Bulletin*, **105**, 251-271.

[13] Robertson, A.H.F., Ustaömer, T., Parlak, O., Ünlügenç, U.C., Taşlı, K. and Inan, N. (2006a) Erratum to the berit transect of the Tauride thrust belt, S Turkey: Late cretaceous-early cenozoic accretionary/collisional processes related to closure of the Southern Neotethys. *Journal of Asian Earth Sciences*, **27**, 108-145. doi:10.1016/j.jseaes.2005.02.004

[14] Robertson, A.H.F., Parlak, O., Rızaoğlu, T., *et al.* (2006b) Late Cretaceous-Mid Paleocene tectonic evolution of the eastern Taurus Maountains and southern Tethyan ocean evidence from the Elazığ region, SE Turkey. *Geological Society*, Special Publication, **272**, 231-270.

[15] Hemton, M.R. and Savcı, G. (1982) Elazığ volkanik karmaşığının petrolojik ve yapısal özellikleri. *Türkiye Jeoloji Kurumu Bülteni*, **25**, 143-150.

[16] Steinitz, G., Lang, B., Mor, D. and Dallal, C. (1983) The K-Ar laboratory at the Geological Survey of Israel. *Israel Geology Survey Current Research*, **19**, 97-98.

[17] Kotlarsky, P., Kapusta, J., Lang, B. and Steınıtz, G. (1992) Calculation of isotopic ratios of argon on the MM-1200 mass-spectrometer at the Geological Survey of Israel. *Isr. Geol. Surv. Rep. TR-GSI*, 17.

[18] Yilmaz, Y. (1990) Comparison of young associations of western and eastern Anatolia formed under compressional regime. *Journal of Volcanology and Geothermal Research*, **44**, 69-87. doi:10.1016/0377-0273(90)90012-5

[19] Ketin, I. (1983) Türkiye jeolojisine genel bir bakış: İ.T.Ü. Kütüphanesi, 595.

[20] Perinçek, D. and Kozlu, H. (1984) Stratigraphy and structural relations of the units in the Afşin-Elbistan-Doğanşehir region (Eastern Taurus). *Geology of the Taurus Belt*. *Proceedings of International Symposium*, MTA, Ankara, 26-29 September 1984, 181-198.

[21] Kipman, E. (1983) Keban volkanitlerinin petrolojisi. İ.Ü. *Yer Bilimleri Dergisi*, **3**, 205-230.

[22] Kaya, A. (2001) Structural analyses and tectonic evolution of the metamorphites in the Keban (Elazığ) vicinity. Firat Üniversitesi Fen Bilimleri Enstitüsü Jeoloji Mühendisliği Anabilim Dali, Doktora Tezi 133s (In Turkish with English abstract).

[23] Yazgan, E. (1983) A geotraverse between the Arabian platforme and the Munzur Nappes. *International Symposium on the Geology of the Taurus Belt Field Guide Book Excursiony*.

[24] Yazgan, E. (1984) Geodynamics evolution of the Eastern Taurus region. *Geology of the Taurus Belt International Symposium*, Ankara, 26-29 September 1984, 199-208.

[25] Ural, M. and Kürüm, S. (2009) Microscopic and diffractometric studies inferred from skarn zonations between the keban metamorphics and elazığ magmatites, around Elazığ, F.Ü. *Turkish Journal of Science*, **4**, 87-102.

[26] Didier, J. and Barbarin, B. (1991) The different types of enclaves in granites-nomenclature: Enclaves and granite petrology. In Didier, J. and Barbarin, B., Eds., *Developments in Petrology*, *Elsevier*, **13**, 19-23.

[27] Barbarin, B. and Didier, J. (1992) Genesis and evolution of mafic microgranular enclaves through various types of interaction between coexisting felsic and mafic magmas. *Transactions of the Royal Society of Edinburgh. Earth Sciences*, **83**, 145-153.

[28] Debon, F. and Le Fort, P. (1983) A chemical-mineralogical classification of common plutonic rocks and asso-

ciations. *Transactions of the Royal Society of Edinburgh. Earth Sciences*, **73**, 135-149.
[29] Hibbard, M.J. (1995). Petrography to petrogenesis. Prentice Hall, 587.
[30] Önal, A. (2008) Baskil granitoyidi'nin K-Ar soğuma yaşı, tüm kayaç ve Pb-Sr izotop jeokimyası. *Jeoloji Kurultayı Bildiri Özleri*, Ankara, **61**, 110-111.
[31] Irvine, T.N. and Baragar, W.R.A. (1971) A guide to the chemical classification of common volcanic rocks. *Canada Journal of Earth Sciences*, **8**, 523-548. doi:10.1139/e71-055
[32] Rickwood, P.C. (1989) Boundary lines within petrologic diagrams which use oxides of major and minor elements. *Lithos*, **22**, 247-263. doi:10.1016/0024-4937(89)90028-5
[33] Le Maitre, R.W., Bateman, P., Dudek, A., *et al.* (1989) A classification of igneous rocks and glossary of terms. Recommendations of the international union of geological sciences subcommission on the systematics of igneous rocks. Blackwell Science Publication, Hoboken, 193.
[34] Manier, P.D. and Piccoli, P.M. (1989) Tectonic discrimination of granitoids. *Geological Society of American Bulletin*, **101**, 635-643. doi:10.1130/0016-7606(1989)101<0635:TDOG>2.3.CO;2
[35] White, A.J.R. and Chappell, B.W. (1988) Some supracrustal (S-type) granites of the Lachlan Fold Belt. *Transactions of the Royal Society of Edinburgh. Earth Sciences*, **79**, 169-181.
[36] Collins, W.J., Beams, S.D., White, A.J.R. and Chappell, B.W. (1982) Nature and origin of A-type granites with particular reference to southeastern Australia. *Contrib Mineral Petrology*, **80**, 189-200. doi:10.1007/BF00374895
[37] Rollinson, H.R. (1993) Using geochemical data: Evaluation, presentation, interpretation. Longman Scientific and Technical, Wiley, New York, 352.
[38] Sun, S.S. and McDonough, W.F. (1989) Chemical andisotopic systematics of oceanic basalts: Implications for mantle composition and processes: Magmatism in the Ocean Basins. In: Saunders A.D. and Norry M.J., Eds., *Geological Society*, Special Publication, **42**, 313-345.
[39] Boztuğ, D., Erçin, A.I., Kuruçelik, M.K., *et al.* (2006) Main geochemical characteristics of the composite Kaçkar batholith derived from the subduction through collision to extensional stages of Neo-Tethyan convergence system in the Eastern Pontides, Turkey. *Journal of Asian Earth Sciences*, **27**, 286-302.
[40] Boztuğ, D. and Satır, M. (2008) Sr-Nd-Pb-isotopic constraints on the genesis of collision-related S-I-A-type granite associations in central Anatolia, Turkey. *The 6th Hutton Symposium on the Origin of Granites and Related Rocks. Earth and Environmental Science Transactions Royal Society of Edinburgh*, **100**, 1-2.
[41] Zindler, A. and Hart, S. (1986) Chemical geodynamics. *Annual Reviews of Earth and Planetary Science*, **14**, 493-571. doi:10.1146/annurev.ea.14.050186.002425
[42] McDougall, I. and Harrison, T.M. (1999) Geochronology and thermo chronology by the 40Ar/39Ar method. Oxford University Press, Oxford.
[43] Köprübaşı, N. and Aldanmaz, E. (2004) Geochemical constrants on the petrogenesis of Cenozoic I-type granitoids in Northwestern Anatolia. Turkey: Evidence for magma generation by lithospheric delamination in a post-collisional setting. *International Geology Reviews*, **46**, 705-729.
[44] Aldanmaz, E., Pearce, J.A., Thirlwall, M.F. and Mitchell, J.G. (2000) Petrogenetic evolution of the late Cenozoic, post-collision volcanism in western Anatolia. Turkey. *Journal of Volcanology and Geothermal Research*, **102**, 67-95. doi:10.1016/S0377-0273(00)00182-7
[45] Keskin, M., Pearce, J.A. and Mitchell, J.G. (1998) Volcano-stratigraphy and geochemistry of collision volcanism on the Erzurum-Kars plateau, Northeastern Turkey. *Journal of Volcanology and Geothermal Research*, **85**, 355-404. doi:10.1016/S0377-0273(98)00063-8
[46] Nicholson, H. and Latin, D. (1992) Olivine tholeiites from Krafla, Iceland: Evidence for variations in melt fraction within a plume. *Journal of Petrology*, **33**, 1105-1124.
[47] Hibbard, M.J. (1991) Textural anatomy of twelve magma-mixed granitoid systems: Enclaves and granite petrology. In: Didier, J. and Barbarin, B., Eds., *Developments in Petrology*, **13**, 431-444.
[48] Machado, A., Lima, E.F., Chemale, F.J., *et al.* (2005) Geochemistry constraints of mesozoic-cenozoic calc- alkaline magmatism in the South Shetland Arc, Antarctica. *Journal of South American Earth Sciences*, **18**, 407- 425. doi:10.1016/j.jsames.2004.11.011
[49] Chappell, B.W. and Stephens, W.E. (1988) Origin of infra crustal (I-type) granite magmas. *Transactions of the Royal Society of Edinburgh. Earth Sciences*, **79**, 71-86.
[50] Ekici, T., Alpaslan, M., Parlak, O. and Temel, A. (2007) Geochemistry of the pliocene basalts erupted along the Malatya-Ovacik fault zone (MOFZ), Eastern Anatolia, Turkey: Implications for source characteristics and partial melting processes. *Chemie der Erde Geochemistry*, **67**, 201-212. doi:10.1016/j.chemer.2006.01.007
[51] Pearce, J.A. (1982) Trace element characteristics of lavas from destructive plate boundaries: Andesites, orogenic andesites and related rocks. In: Thorpe, R.S., Ed., Wiley, Chichester, pp. 525-548.
[52] Alpaslan, M., Yılmaz, H. and Temel, A. (2004) Geochemistry of post-collision Pliocene-Quaternary Karasar basalt (Divriği-Sivas, esatern Turkey): Evidence for partial melting processes. *Geologica Carpathica*, **55**, 487-500.
[53] Pearce, J.A., Bender, J.F., De Long, S.E., *et al.* (1990) Genesis of collision volcanism in Eastern Anatolia, Turkey. *Journal of Volcanology and Geothermal Research*, **44**, 189-229. doi:10.1016/0377-0273(90)90018-B
[54] Jahn, B.M., Wu, F., Lo, C.H. and Tsai, C.H. (1999) Crust-mantle interaction induced by deep subduction of the continental crust: Geochemical and Sr-Nd isotopic evidence from post-collisional mafic-ultramafic intrusions of the northern Dabie complex, central China. *Chemical Geology*, **157**, 119-146. doi:10.1016/S0009-2541(98)00197-1
[55] Carlson, R.W. and Hart, W.K. (1988) Flood basalt volcanism in the Pacific North-western United States: Continental flood basalts. 35-62.
[56] De Paolo, D.J. (1981) Trace element and isotopic effects of combined wall rock assimilation and fractional crystallization. *Earth and Planet Science Letters*, **53**, 189-202. doi:10.1016/0012-821X(81)90153-9
[57] Stern, R.J. (2002) Subduction zones. *Reviews of Geo-*

physics, **40**, 1012. doi:10.1029/2001RG000108

[58] Fitton, J.G., James, D. and Leeman, W.P. (1991) Basic magmatism associated with Late Cenozoic extension in the western United States: Compositional variation in space and time: The temporal and spatial association of magmatism and metamorphic core complexes. *Journal of Geophysical Research*, **96**, 693-711. doi:10.1029/91JB00372

[59] Kelemen, P.B., Johnson, K.T.M., Kinzler, R.J. and Irving, A.J. (1990) High-field-strength element depletions in arc basalts due to mantle-magma interaction. *Nature*, **345**, 521-524. doi:10.1038/345521a0

[60] Villemant, B., Jaffrezic, H., Joron, J.L., *et al.* (1981) Distribution coefficients of major and trace elements: Fractional crystallization in the alkalibasalt series of Chaine du puy (Massif Central, France). *Geochim Cosmochim Acta*, **45**, 1997-2016. doi:10.1016/0016-7037(81)90055-7

[61] Perinçek, D. (1979) The geology of Hazro-Korudağ-Çüngüş-Maden-Ergani-Hazar-Elazığ-Malatya area. *Türkiye Jeoloji Kurumu Yayını*, 33.

[62] Pearce, J.A., Harris, N.B.W. and Tindle, A.G.W. (1984) Trace element discrimination diagrams for the tectonic interpretation of granitic rocks. *Journal of Petrology*, **25**, 956-983.

[63] Yalınız, K.M., Aydın, N.S., Göncüoğlu, M.C. and Parlak, O. (2000) Terlemez quartz monzonite of the central Anatolia (Aksaray-Sarikaraman): Age, petrogenesis and geotectonic implications for ophiolite emplacement. *Geological Journal*, **34**, 233-242.

[64] Robertson, A.H.F. (2006) Field-based evidence from the south Mediterranean region (Crete, Peloponnese, Evia, Sicily) used to test alternative models for the regional tectonic setting of Tethys during late Palaeozoic-early Mesozoic time: Tectonic development of the Eastern Mediterranean Region. In: Robertson, A.H.F. and Mountrakis, S., Eds., *Geological Society*, Special Publication, **210**, 91-154.

[65] Parlak, O., Höck, V., Kozlu, H. and Delaloye, M. (2004) Oceanic crust generation in an island arc tectonic setting, SE Anatolian Orogenic Belt (Turkey). *Geological Magazine*, **141**, 583-603. doi:10.1017/S0016756804009458

[66] Pearce, J.A. (1983) Role of the subcontinental lithosphere in magma genesis at continental margins: Continental basalts and mantle xenoliths. In: Hawkesworth, C.J. and Norry, M.J., Eds., Shiva Publishing, Cheshire, 230-249.

